Additive Manufacturing 53 (2022) 102689

Contents lists available at ScienceDirect

Additive Manufacturing

journal homepage: www.elsevier.com/locate/addma

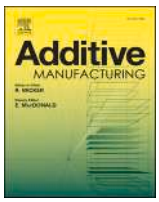

4D printing of multiple shape memory polymer and nanocomposites with biocompatible, programmable and selectively actuated properties

Xue Wan [a], Yang He [a], Yanju Liu [b], Jinsong Leng [a,*]

[a] Center for Composite Materials and Structures, Harbin Institute of Technology (HIT), No. 2 Yikuang Street, P.O. Box 3011, Harbin 150080, People's Republic of China
[b] Department of Astronautical Science and Mechanics, Harbin Institute of Technology (HIT), P.O. Box 301, No. 92 West Dazhi Street, Harbin 150001, People's Republic of China

ARTICLE INFO

Keywords:
4D printing
Shape memory polymer
Multiple shape memory
Magnetic field
Biocompatible

ABSTRACT

4D printing of shape memory polymers (SMPs) endows the 3D printed structures with tunable shape-changing behavior and functionalities that opens up new avenues towards intelligent devices. Multiple-SMPs, specially, could memorize more than two shapes that have greatly extended the performance of 4D printed structures. However, the actuation to trigger the shape change of 4D printed multiple-SMPs is usually by direct heating to different temperatures. It hasn't brought the full superiority of the programmability of multiple-SMPs with distinct responsive regions that could be sequentially and selectively actuated by various stimuli. Besides, the functionality of multi-material based additive manufacturing is another area that has not been fully developed. Herein, 4D printing of poly (D,L-lactide-co-trimethylene carbonate) (PLMC)/poly (trimethylene carbonate) (PTMC)/Fe_3O_4 multi-material with multiple shape-changing capabilities under sequential stimuli of remotely magnetic field and heat was achieved. At first, we optimized the composition of pure SMP to fine tune the multiple shape memory effect and quantitatively characterized the shape recovery by stepwise heating. Then with the addition of Fe_3O_4 nanoparticles, the multi-material distribution of 4D printed structure consisting of multiple-SMP and its nanocomposites was designed. The integration of multi-material additive manufacturing with multiple shape memory effect extends the shape transformation to quintuple complex shapes with accurate and local controllability under selective multi-stimuli. The 4D printed multiple-SMP and its nanocomposites with simultaneously thermo- and magnetic- responsive shape-changing capability also demonstrated excellent biocompatibility. This work thus offers a feasible and robust approach for 4D printing of multi-functional devices for broad applications in entertainment, robotics, biomedical field and beyond.

1. Introduction

The additive manufacturing technique, also known as three-dimensional (3D) printing, has attracted a lot of attention in various fields including tissue engineering, electronics, robotics and aerospace engineering [1–4]. Evolved from 3D printing, four-dimensional (4D) printing is a newly developed fabricating technique that converges additive manufacturing and shape-morphing smart materials into an innovation platform [5,6]. 4D printing enables the 3D printed structures to actively change their configurations or functionalities over time under an external stimulus [7–11]. As an important kind of smart materials, shape memory polymer (SMP) possesses the shape-changing property from a programmed temporary shape to its original shape under specific stimuli, including heat, electricity, light, magnetic field, etc [12–15]. Owing to their light weight, large deformation and easy processability, SMPs have shown great promise in myriad applications, including aerospace field [16,17], robotics [18,19], electronics [20] and biomedical field [21]. The development of 4D printing endows 3D printed SMPs with not only customer-designed structures, but also complex deformation modes based on structural designs [22,23].

Most SMPs are dual-shape memory polymers with a single transition temperature (responding to the glass or melting transition) that could only memorize one temporary shape [24,25]. Recently, more and more researchers concentrate on multiple-shape memory polymers (multiple-SMPs) with multi-transition temperatures which could memorize more than two shapes, thus broadening their functionality to meet different application needs [26,27]. Triple-shape memory polymers (triple-SMPs) are the most common multiple-SMPs, which can be

* Corresponding author.
E-mail address: lengjs@hit.edu.cn (J. Leng).

https://doi.org/10.1016/j.addma.2022.102689
Received 8 December 2021; Received in revised form 7 February 2022; Accepted 13 February 2022
Available online 17 February 2022

prepared by two main routes to realize the triple-shape memory effect. One is the preparation of a broad thermal transition area [26,28–30], while the other is a manipulation of two discrete thermal transitions [31–33]. Besides, the single broad thermal transition could be considered as a collection of several discrete thermal transitions. It is worth noting that except for these two methods, sequential two-stage programming is also an efficient method to realize sequential shape recovery upon heating [34,35]. Because this does not belong to the traditional concept of multiple-SMPs, this is not the main point here. So far, some work concerning 3D and 4D printing of multiple-SMPs has been reported. For example, Li et al. fabricated extrinsic multiple-SMPs consisting of tri-block copolymers and the multiple-shape memory effect relied on macroscale spatio-assembly rather than molecular design [36]. They utilized the fused deposition modelling (FDM) technique to integrate several individual transition phases into a printed structure to exhibit intermediate temporary shapes upon continuous heating. Unlike the extrinsic method, Chen et al. prepared multiple-SMPs consisting of three thermoplastic polymers with multiple-shape memory effect and fed them into an FDM printer to construct smart objects [37]. However, the stimulus to trigger sequential shape changes of the printed multiple-SMPs is limited to the single direct heating, which restricts the number and complexity of shape deformations of multiple-SMPs. For example, multiple-SMPs are capable of changing more complex shapes by remote triggering under selective magnetic and electric fields [31]. Besides, multi-material printing enables the integration of individual parts with various deformation forms into one structure [38]. So far, it hasn't brought the full superiority of integrating both the programmability of multiple-SMPs and multi-material design with different stimuli-responsive regions to realize sequential and selective actuation. , Therefore, 4D printed multiple-SMPs with controllable shape change under selective multi-stimuli and more complex deformation forms are highly desired in the face of ever-increasing multifunctional demands.

In this study, we 4D printed a biocompatible multiple-SMP and its nanocomposites containing Fe_3O_4 nanoparticles by direct ink writing (DIW) technique combined with multi-material printing. Compared to other printing technique, DIW possesses the advantages of wide choice of materials type, open-source apparatus, convenient parameters setting, low consumption of materials, exchangeable barrels, flexible choice of various nozzles and easy design of multi-material printing [39,40]. Unlike conventional printed multiple-SMP which is overall responsive to heat, herein, the 4D printed multi-material structures could exhibit selective and programmable shape transformation as only the parts containing Fe_3O_4 are sensitive to an alternating magnetic field. Under selective stimuli of heat and remotely magnetic field, the 4D printed multi-material structures exhibit sequential and complicated shape transformations with good multiple-shape memory effect and good biocompatibility, showing great promise towards the applications of entertainment, robotics, biomedical field and beyond.

2. Material and methods

2.1. Materials

PLMC and PTMC were bought from Jinan Daigang Corporation. The monomeric molar ratio of D,L-lactic acid to trimethylene carbonate in PLMC was 80:20. Dichloromethane (DCM) and Fe_3O_4 nanoparticles with an average diameter of 30 nm were purchased from Aladdin Industrial Corporation and directly used.

2.2. Preparation of the thermo- and magnetic-responsive printable inks

The PLMC/PTMC blends with varied feed ratios of 33/67, 50/50, 67/33, 80/20 and 90/10, were dissolved adequately in DCM. The ink of PLMC/PTMC for 4D printing was prepared by dissolving the two materials PLMC/PTMC (50/50) in DCM in a mass fraction of 1/6, denoted as Ink 1. The nanocomposites ink was prepared by adding Fe_3O_4, with the weight ratio of PLMC:PTMC:Fe_3O_4:DCM at 1:1:0.5:40 in an open container so that DCM could evaporate. When the mass fraction was 1/6, the container was sealed and labeled as Ink 2.

2.3. Ink rheological test

Both Ink 1 and 2 were centrifuged to remove bubbles before testing. A diameter of 25 mm and an angle of 2 °cone-plate geometry was utilized for rheology test by a DHR-2 rotary rheometer (TA Instruments) at 25 ℃. The viscosity was tested over the shear rate in the range of 0.01–200 s^{-1}. The oscillation amplitude mode was adopted with escalating shear strain from 0.001% to 500% at a frequency of 1 Hz. Each ink was tested three times.

2.4. 3D printing

The printed structures were constructed by a 3D-Bioplotter™ (EnvisionTEC GmbH, Germany). Ink 1 or 2 was transferred into a 30 cc cartridge mounted on the low-temperature dispensing head. The printing parameters of each structure were listed in Table S1 (Supporting Information). The ink was printed from the micro nozzle under applied air pressure. Various customized structures were printed by adjusting the printing parameters including the nozzle size, applied pressure and robot velocity. Some structures were folded into more complicated structures by origami after they were printed. The new folded shape was fixed in a mold to reshape its permanent shape during full solvent evaporation. All the printed structures were further dried in a 50 ℃ vacuum oven for 12 h to fully remove the solvent.

2.5. Shape memory effect measurement

The shape memory properties were characterized using the controlled force mode by DMA Q800 [26,41]. The shape fixity ratio (R_f) along with shape recovery ratio (R_r) for dual-shape memory effect from shape "0" to "1", were calculated as follows:

$$R_{f1} = \frac{\varepsilon_1}{\varepsilon_{1,load}} \times 100\% \quad (1)$$

$$R_{r1} = \frac{\varepsilon_1 - \varepsilon_{0,rec}}{\varepsilon_1 - \varepsilon_0} \times 100\% \quad (2)$$

where $\varepsilon_{1,load}$ is the deformed strain under external force, ε_1 represents the fixed strain, $\varepsilon_{0,rec}$ denotes to the recovered strain after reheating and ε_0 denotes to the initial strain in each cycle. For the triple-shape memory effect, the cycle was performed at two deformation temperatures (T_{d1} and T_{d2}) and shape memory properties were calculated by Eqs. (1) to (4). From shape "1" to "2", R_f and R_r were calculated as follows:

$$R_{f2} = \frac{\varepsilon_2 - \varepsilon_1}{\varepsilon_{2,load} - \varepsilon_1} \times 100\% \quad (3)$$

$$R_{r2} = \frac{\varepsilon_2 - \varepsilon_{1,rec}}{\varepsilon_2 - \varepsilon_1} \times 100\% \quad (4)$$

where ε_2 and $\varepsilon_{2,load}$ denote to the fixed strain and deformed strain at shape "2", respectively. $\varepsilon_{1,rec}$ is the recovered strain at shape "1". Each sample was measured three samples.

2.6. Cell culture

NIH/3T3 cell lines were cultured in Dulbecco's Modified Eagle's Medium which was supplemented with 10% (v/v) fetal bovine serum and 1% (v/v) penicillin-streptomycin at 37 °C. When the NIH/3T3 cells reached confluence, they were trypsinized using 0.05 (w/v) trypsin−EDTA and added into 96-well plates for further characterization.

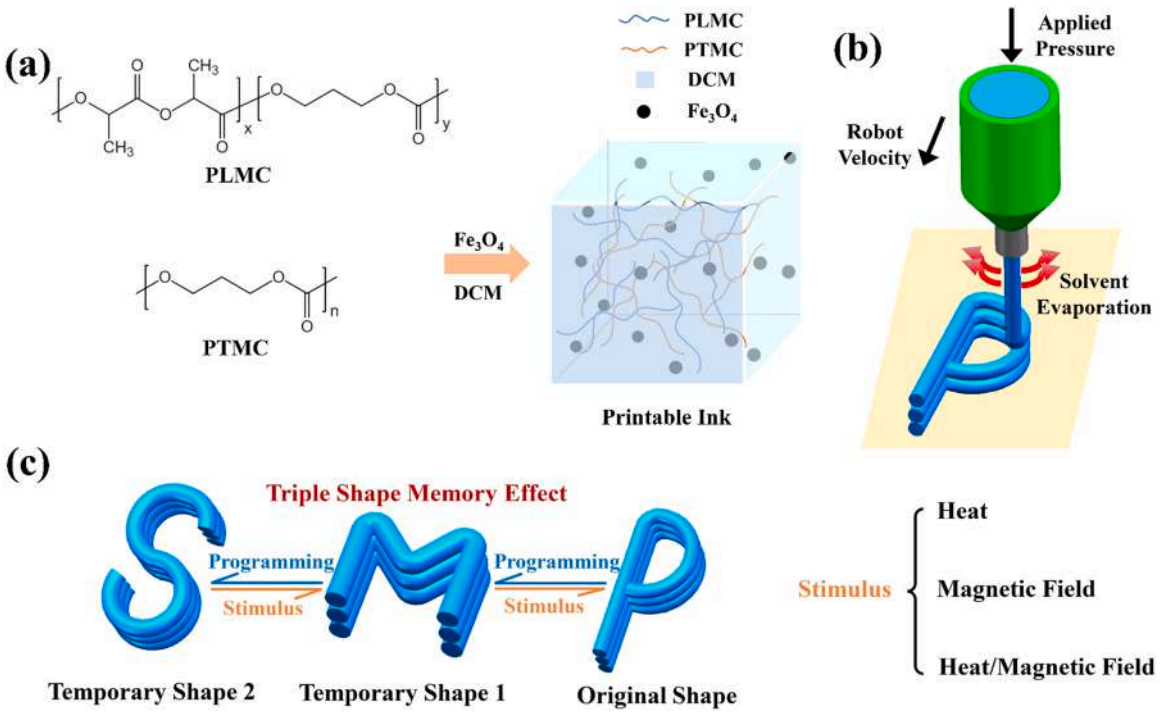

Fig. 1. Schematic illustration of 4D printing of triple shape memory PLMC/PTMC/Fe_3O_4. (a) Composition of the printable nanocomposites ink. (b) Schematic 3D printing process. (c) Shape-changing behavior based on triple shape memory effect of the 4D printed structure under an external stimulus of heat, magnetic field or both.

2.7. Cell proliferation

The 3D printed monolayer PLMC/PTMC film was sterilized with 75% EtOH and then dissolved in DMSO at various concentrations (0.05, 0.1 and 0.2 mg mL^{-1}). The blank group and DMSO group were also chosen as a contrast. NIH/3T3 fibroblast cells were collected and 1×10^3 cells

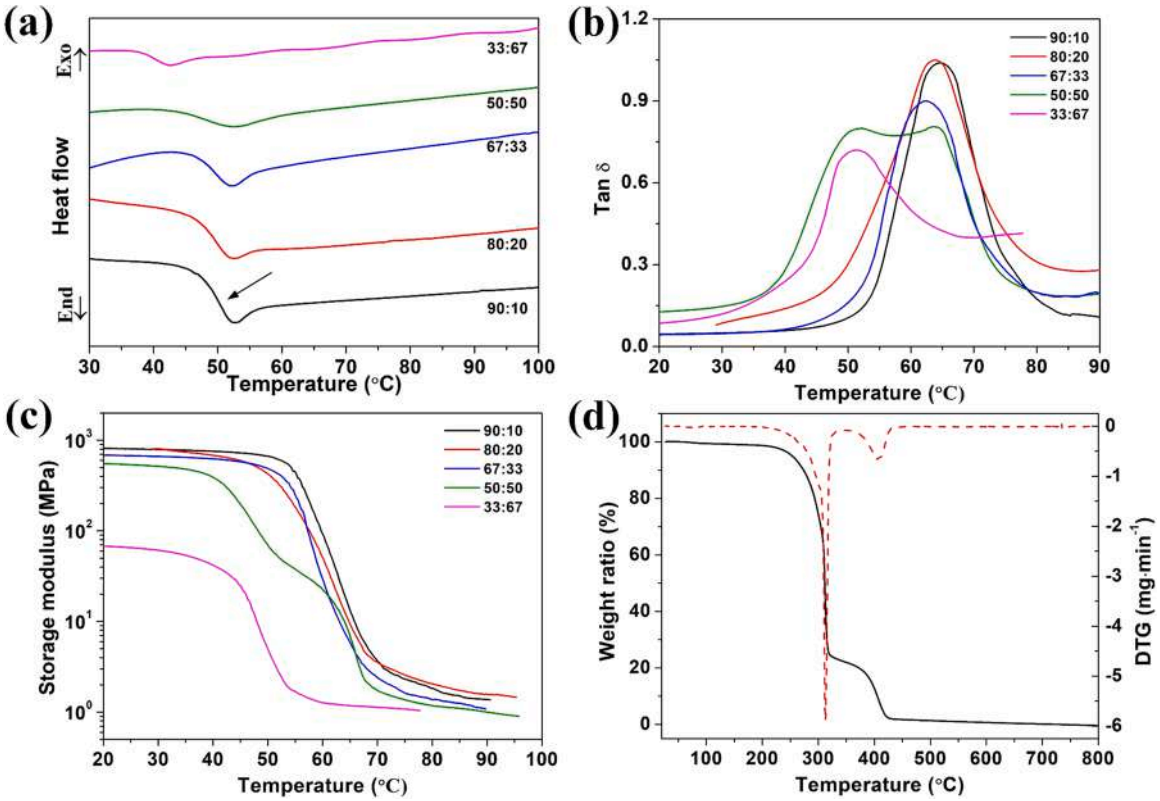

Fig. 2. Thermal properties of PLMC/PTMC blend with various weight ratios. (a) DSC thermogram; (b) tan δ and (c) Storage modulus versus temperature curve; (d) TGA and DTG plots versus temperature.

Table 1
Thermal properties of the PLMC/PTMC blends.

Mass ratio of PLMC/PTMC	T_g by DSC (℃)	T_g by DMA (℃)
0:100	-10.06	–
33:67	40.10	51.05
50:50	47.22	51.86, 63.73
67:33	48.65	62.39
80:20	49.28	63.78
90:10	49.80	64.61
100:0	49.97	–

were seeded in 96-well plates containing materials. Cell proliferation test was assessed using a CCK-8 cell proliferation kit (Beyotime Institute of Biotechnology, China) on days 1, 2 and 3 after incubation. After incubation for another 4 h, the absorbance at 450 nm was read by a Bio-Rad microplate reader.

2.8. Live/Dead staining

The 3D printed shape memory PLMC/PTMC and its nanocomposites were sterilized in 75% EtOH. Removed cells were seeded at a density of 1×10^6 cells in 2 mL of complete growth medium and incubated at 37 °C in a fully-humidified atmosphere of 5% CO_2 in air with daily media changed. After seeding for 48 h, unattached cells were removed by aspirating the medium and the materials were rinsed 3 times with 2 mL PBS. Then the cell vitality of materials was evaluated with a LIVE/DEAD® Viability/Cytotoxicity Kit (ThermoFisher). The random five fields were chosen and the images were taken using a Leica microscope.

3. Results and discussion

Fig. 1 shows the schematic illustration of 4D printing of shape memory PLMC/PTMC blend and its nanocomposites containing magnetic nanoparticles, Fe_3O_4. The PLMC/PTMC blend served as a matrix with triple shape memory effect for shape change under the thermal stimulus. Fe_3O_4 served as magnetic-responsive sources to endow the matrix with shape change in an alternating magnetic field [31]. The mixture is dispersed in DCM, a volatile solvent to prepare printable ink, as illustrated in Fig. 1(a). The ink is then transferred into a barrel to construct structures through layer-by-layer deposition under applied

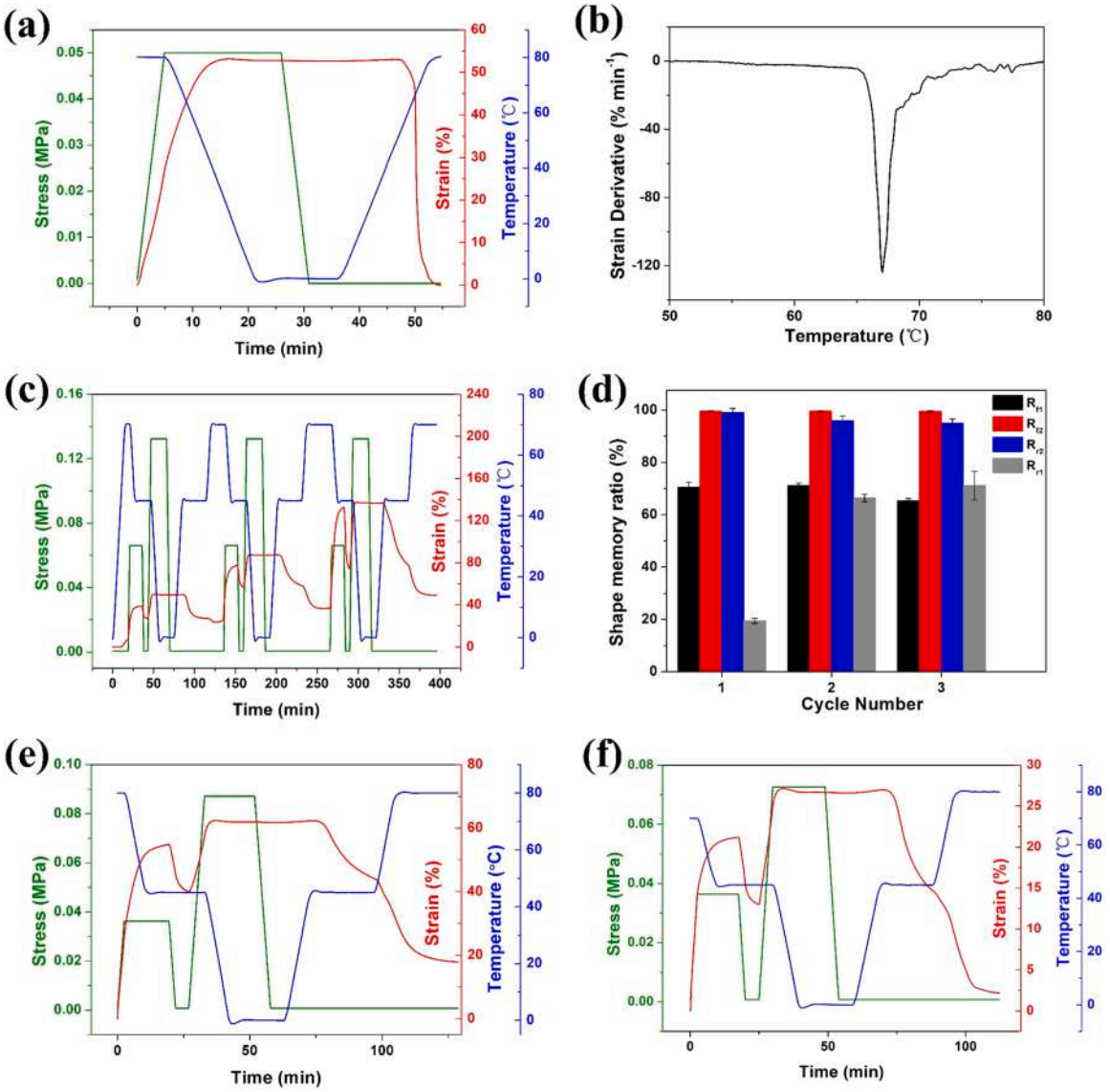

Fig. 3. Quantitative shape memory properties of the PLMC/PTMC (50:50). (a) Dual shape memory cycle (T_d= T_r =80 ℃). (b) Strain derivative curve of the dual shape memory cycle. (c) Three consecutive triple shape memory cycles ($T_{d1} = T_{r2}$ = 70 ℃, $T_{d2} = T_{r1}$ =45 ℃). (d) Quantitative triple shape memory ratios. (e) The third triple shape memory cycle ($T_{d1} = T_{r2}$ =80 ℃, $T_{d2} = T_{r1}$ =45 ℃). (f) The third triple shape memory cycle (T_{d1} = 70 ℃, $T_{d2} = T_{r1}$ =45 ℃, T_{r2} =80 ℃).

pressure, as shown in Fig. 1(b) and Movie S1 (Supporting Information). The thermo-responsive PLMC/PTMC blend endows the printed structure with triple shape memory behavior. Fig. 1(c) illustrates that by programming the 3D printed structure into two different temporary shapes continuously under uniform temperatures, it would recover sequentially under external stimuli of heat, magnetic field or a combination of heat and magnetic field.

3.1. Optimization of the thermo-responsive triple SMP

Fig. 2 depicts the thermal properties of the shape memory PLMC/PTMC blend. The DSC curve shown in Fig. 2(a) reflects the matrix behaved amorphous because only one endothermic peak appeared. The step where the arrow points to corresponds to the glass transition and their respective glass transition temperatures (T_gs) are recorded in Table 1 and Fig. S1. The T_g decreased as the weight ratio of PLMC/PTMC decreased, indicating that the introduction of PTMC enhanced the mobility of molecular chains. The smooth endothermic peak revealed that the two polymers had good compatibility. The T_gs were also characterized by the peak of damping factor (tan δ) in the DMA curve as shown in Fig. 2(b). With an increase of the content of PTMC, the α-relaxation shifted to a lower T_g with a reduction of the height of tan δ, in agreement with previous studies [28]. Interestingly, the PLMC/PTMC (50:50) splitsinto two T_gs, with the broadest glass transition region in accordance with the "self-concentration model" [42]. When the mass fraction of PTMC accounted for half of the blend, it may cause microphase separation. The two split T_gs were a little bit close, thus the respective regions of glass transition overlapped. The difference between DSC and DMA tests was because the principles of these two methods were different. DMA is more sensitive than DSC because it could detect mechanical motions of molecule chains in short range while DSC records changes in the heat capacity [43]. Thus, DSC is not as distinguishable and accurate as DMA when detecting thermal transitions. The T_gs characterized by DMA were higher than that of DSC due to the hysteresis of the movement of polymer segments in DMA [44]. When PLMC and PTMC were mixed together, the inhomogeneous molecular entanglement during the DMA test was magnified thus the microphase separation occurred apparently at the weight ratio of 50:50. The broad glass transition range created the possibility of multiple shape memory when the deformation and recovery temperatures were set within this region [26,29]. Fig. 2(c) records the variation of storage modulus and the 50:50 blend had two areas where the modulus dropped rapidly (40–50 ℃ and 60–70 ℃). The stepwise decrease in storage modulus could release the fixed strain at two deformation temperatures, resulting in triple shape memory behavior [32]. The thermogravimetric curve of PLMC/PTMC (50:50) demonstrated in Fig. 2(d) shows two thermal decomposition regions, which correspond to the polymer chain cleavage. The mass loss dropped to a plateau at ~ 25%, which also reflected that a slight microphase separation phenomenon existed in the system. The symmetric blend possessed a decomposition temperature (T_d) at 273.7 ℃, defined as the temperature value with a mass loss of 10%. Based on the above results and the evidence of the most effective triple SMP [28], the symmetric blend in a weight ratio of 50:50 was chosen to further test the shape memory behavior. As seen from Fig. S2 (Supporting Information), the strong peak at 1745, 1183 and 1180 cm^{-1} of PLMC/PTMC (50:50) was assigned to C═O, C—C and C—C stretching vibration peak, respectively. The PLMC/PTMC/Fe_3O_4 nanocomposites showed a characterized Fe–O peak at 568 cm^{-1}. The slight shift of -C═O peak of nanocomposites may attribute to the interaction of C═O bond with Fe atoms [45].

3.2. Triple shape memory and mechanical properties of thermo-responsive SMP

Fig. 3(a) depicts the dual shape memory cycle of the PLMC/PTMC (50:50) blend. The sample was uniaxially elongated at 80 ℃ followed by cooling and load removal to fix the strain. The subsequent recovery was observed under continuous reheating at a rate of 5 ℃ min^{-1}. The R_f and R_r calculated by Eqs. (1) and (2) were 99.8% and 100.0%, respectively. The switch temperature (T_{sw}) was defined as the inflection point temperature of the maximal shape recovery rate in continuous heating [28]. In Fig. 3(b), the strain derivative reveals a T_{sw} at 67 ℃, close to the deformed temperature (80 ℃). This phenomenon was in agreement with the "temperature memory effect" reported by earlier studies [46–48]. For triple shape memory tests, the deformation (T_{d1} and T_{d2}) and recovery temperatures (T_{r1} and T_{r2}) were chosen at 45 and 70 ℃ according to the results of Fig. 2(c). Fig. 3(c) shows three continuous shape memory cycles and the shape fixity and recovery ratios calculated from Eqs. (1) to (4) are listed in Fig. 3(d) and Table 2. In these shape memory cycles, R_{f1} was only around 70% because the deformed shape was fixed at a relatively high temperature of 45 ℃. R_{f2} was close to 100% due to a low fixed temperature at 0 ℃, which froze the motion of polymer chains more thoroughly. Similarly, the value of R_{r2} approached 100% as the sample recovered most of the strain during the first heating process. The value of R_{r1} in the first cycle was only 19.19%, which was attributed to the intrinsic characteristics of common SMPs [49]. With the increase of cycle number, R_{r1} stabilized at ~67%. It is worth pointing out that due to the relatively weak interaction inherent in physical crosslinking networks, thermoplastic multiple SMPs do not have as good shape memory properties as thermoset multiple SMPs. This R_{r1} was similar to reported triple SMPs in the range of 33–80% due to the inefficiency of the physical crosslinking points and the relaxation of polymer chains especially after several cycles [27,28,41]. Then we changed the T_{d1}= T_{r2} at 80 ℃ as a contrast and the third representative shape memory cycle and the calculated results are shown in Fig. 3(e) and Table 2. R_{f1} increased because the temperature interval between T_d and T_r increased, thus the deformed shape could be more adequately fixed. The recovery process was more evident characterized by plotting the strain derivative curve as shown in Fig. S3 (Supporting Information). Two obvious maximum instantaneous recovery rates were clearly observed near the deformed temperatures. The shape memory cycle illustrated in Fig. 3(f) was performed using the same programming steps as in Fig. 3(c) except for T_{r2} = 80 ℃. By this simple method, R_{r1} increased to 83.07% and the calculated data are summarized in Table 2. It revealed that by increasing the temperature of T_{r2}, the value of R_{r2} could increase to some extent. We also examined the triple shape memory properties of the PLMC/PTMC (80:20) as a contrast (Fig. S4, Supporting Information). It could be found that the binary system at this weight ratio also had obvious triple shape memory properties. Because of a narrower region of α-relaxation, the shape recovery ratio of the 80:20 blend was slightly lower than that of the 50:50 blend, which attributed to the "self-concentration model" [42]. Meaningfully, this binary blend in different weight ratios both showed triple shape memory effect, reflecting the broad applicability of this material blend. Fig. S5 (Supporting Information) depicts the static tensile stress-strain curves of PLMC/PTMC at different ratios and all the samples showed elastic-plastic behavior. As the ratio of PLMC/PTMC decreased, the elongation at break increased while the tensile strength and elastic

Table 2
Triple shape memory properties of binary PLMC/PTMC blends.

PLMC/PTMC	Cycle number	T_{d1} = T_{r2} (℃)	T_{d2} = T_{r1} (℃)	R_{f1} (%)	R_{f2} (%)	R_{r2} (%)	R_{r1} (%)
50:50	1	70	45	69.04	99.73	99.42	19.19
	2	70	45	72.15	99.70	95.29	40.53
	3	70	45	64.58	99.36	93.66	67.07
50:50	3	80	45	82.19	99.54	80.50	55.32
	3	T_{d1} = 70, T_{r2} = 80	45	71.93	99.64	87.69	83.07
80:20	3	70	45	58.33	99.76	99.52	59.47

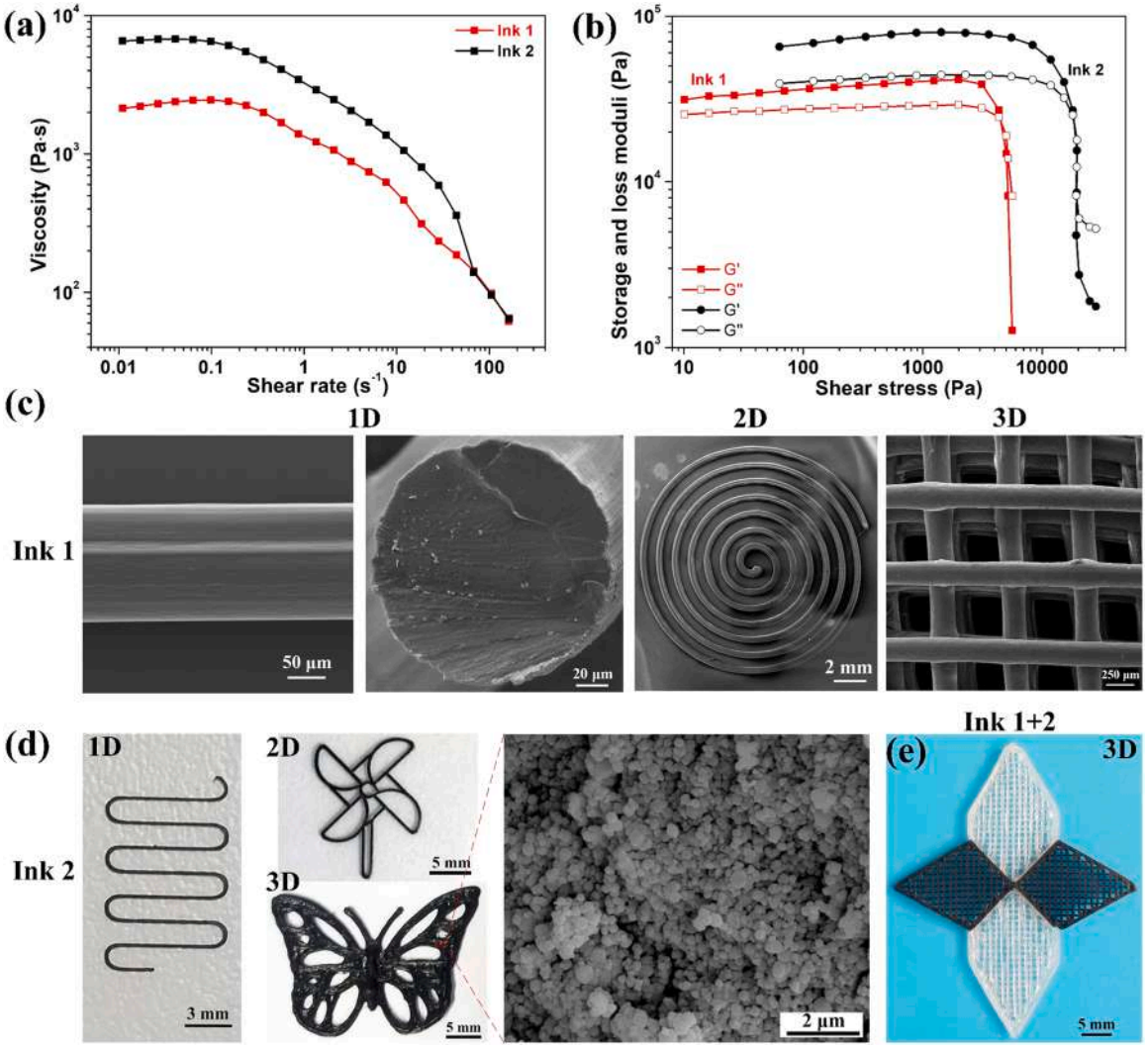

Fig. 4. Printability of PLMC/PTMC (Ink 1) and PLMC/PTMC/Fe_3O_4 nanocomposites (Ink 2). (a) Rheological properties of apparent viscosity over shear rate. (b) Rheological properties of shear storage and loss moduli over shear stress. (c) SEM images of printed structures by Ink 1. (d) Representative structures and the magnified cross-section of the nanocomposites printed by Ink 2. (e) A multi-material structure printed by a combination of Ink 1 and 2.

modulus decreased. It reflected that by tuning the weight ratio of these two polymers, the tunable static mechanical property could be realized. The details are recorded in Table S2 (Supporting Information).

3.3. 3D printing of thermo- and magnetic-responsive SMP inks

Since the PLMC/PTMC (50:50) blend showed excellent better shape memory properties, we dissolved it in DCM to prepare Ink 1 and with the addition of 20 wt% Fe_3O_4 as Ink 2 for 3D printing. Fig. 4(a) depicts the change of viscosity over the shear rate of the two inks. The obvious shear-thinning behavior reflected that the inks met the requirements of extrusion-based 3D printing [50]. The introduction of magnetic particles enhanced the viscosity of the ink, thus increasing the ability of shape retention. The variation of storage and loss moduli of the inks are shown in Fig. 4(b). From the intersection of the moduli curves, we found the yield stress of Ink 2 was almost an order of magnitude higher than that of Ink 1. The addition of Fe_3O_4 endowed Ink 2 with higher shear elastic modulus and higher yield strength to preserve the printed filamentary shape. After modulating the ink viscosity, we exhibited some representative printed examples of both the two inks. Fig. 4(c) shows a series of printed structures from 1D to 3D using Ink 1. The diameter of the 1D filament is around 160 μm and the cross-section of the fracture surface is round and smooth, which laid a good foundation for more complicated structures. The 2D symmetric helix and 3D self-supporting scaffold with multiple layers also proved the good printability of Ink 1. The printed structures of 1D zigzag pattern, 2D windmill and 3D butterfly printed by Ink 2 are demonstrated in Fig. 4(d). All these printed architectures showed high printing fidelity and universality to construct structures from 1D to 3D, micro to macro size, pure polymer to composite. The SEM image of the cross-sectional printed magnetic composite in Fig. 4(d) manifests that Fe_3O_4 nanoparticles were uniformly dispersed in the polymer blend with no obvious agglomeration. The SEM images obtained in other zones shown in Fig. S6 also prove the uniform dispersion of the nanoparticles. We prepared a series of Fe_3O_4/matrix inks with mass content from 5 to 20 wt% and printed them into a scaffold structure. Fig. S7 shows the magnetic-triggered shape recovery process of these composite structures put inside the coil of an alternating magnetic field of 30 kHz. The 5 wt% nanocomposites couldn't recover because of the low inductive heating efficiency. When the content of Fe_3O_4 increased from 10 to 20 wt%, the total shape recovery time decreased from 70 to 60 s. When the mass content was higher than 20 wt%, it was hard to get good printing quality due to the clogging of the nozzle. Hence, we chose a Fe_3O_4 content of 20 wt% which could be easily actuated by an alternating magnetic field of 30 kHz [51]. By exchanging the ink cartridge, a multi-material planar crane printed by a combination of Ink 1 and 2 shown in Fig. 4(e) demonstrated the superior

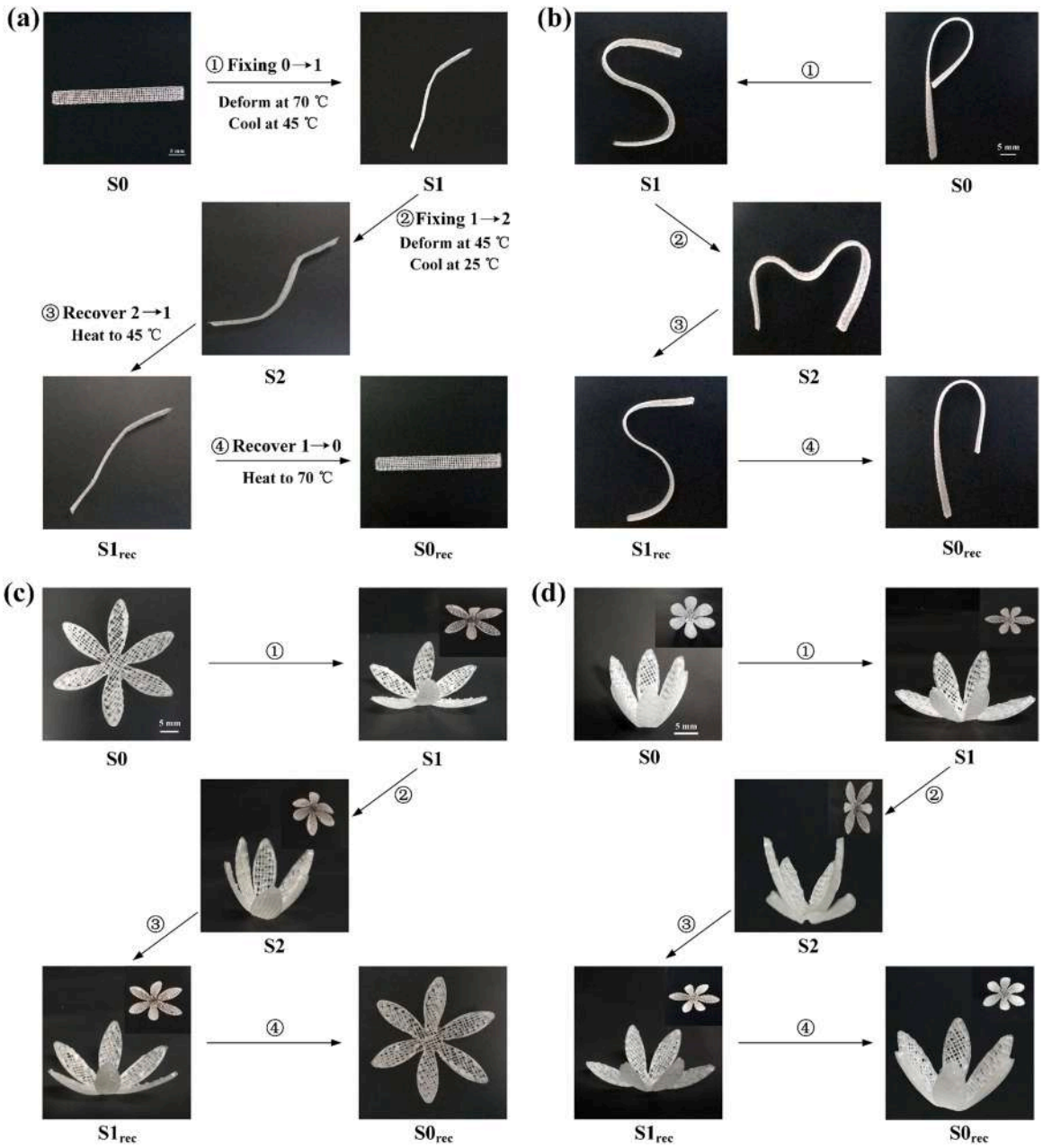

Fig. 5. Triple shape memory process of a 4D printed (a) scaffold; (b) Latin letter; (c) flat flower with six petals and (d) folded flower with six petals under heat stimulus.

flexibility of multi-material 3D printing. Besides, the introduction of Fe_3O_4 had enhancement on both tensile strength and elastic modulus with an increase by 31.4% and 58%, respectively as shown in Fig. S8 and Table S2 (Supporting Information).

3.4. Triple shape transformation of 4D printed thermo-responsive SMP

Based on the quantitative shape memory properties and good printability of both PLMC/PTMC and PLMC/PTMC/Fe_3O_4, we further studied the shape recovery behavior of the printed structures under heat stimulus as shown in Fig. 5. Following were the steps taken: first, the printed structure (original shape, S0) was immersed in a water bath at 70 ℃ followed by deforming into a new shape under an external force. Cooled down the structure to 45 ℃ while maintaining the force and this new temporary shape was denoted as S1. Afterwards, the new shape S1 was programmed into another temporary shape at 45 ℃. Then it was cooled down to 25 ℃ while holding the external force and the new shape was recorded as S2. Upon reheating to 45 and 70 ℃, the scaffold recovered to $S1_{rec}$ and $S0_{rec}$ successively. The scaffold (Fig. 5(a)) was programmed into two temporary shapes with both two ends bent in sequence. The printed Latin letter of "P" was programmed sequentially into the shape of "S" and "M" and the shape change occurred in turn as demonstrated in Fig. 5(b). Fig. 5(c) shows that the printed flat flower with different petals folded recovered to its previous temporary and original shape in sequence. The folded flower (Fig. 5(d)) was deformed into two intermediate states where some petals open while some closed. Upon continuous reheating, the flat flower changed its shape in sequence. From these demonstrations, we found that all the printed structures exhibited an obvious triple shape memory effect and complicated shape transformation between various topological shapes could be easily manipulated. Although some permanent shapes did not recover fully, these examples reflected their continuous shape-changing

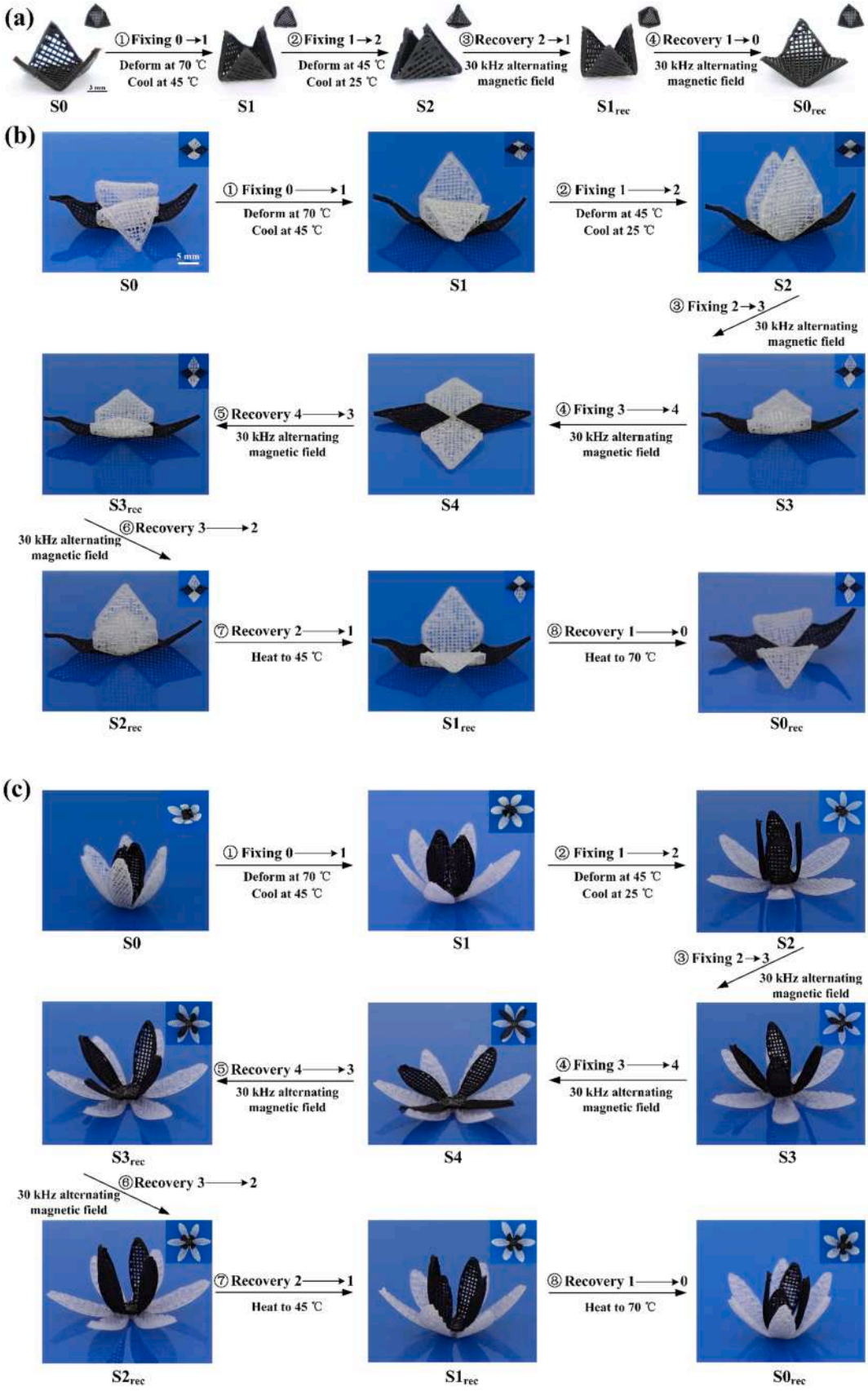

Fig. 6. Multiple and selective shape transformation of a 4D printed (a) tetrahedron under a 30 kHz alternating magnetic field; (b) multi-material crane and (c) multi-material flower under the alternating magnetic field and then immersed in a water bath.

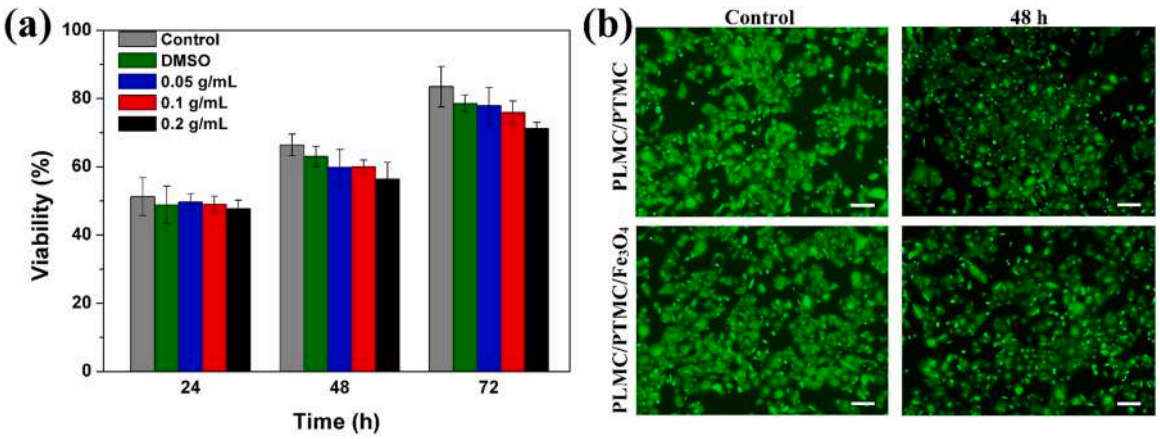

Fig. 7. Biological test results. (a) Cell viability of NIH/3T3 fibroblast cells cultured for 1, 2 and 3 days in extract medium from 3D printed PLMC/PTMC. (b) Fluorescence image of NIH/3T3 cells with 3D printed PLMC/PTMC and PLMC/PTMC/Fe_3O_4 in 48 h. Green and red color correspond to live and dead cells, respectively (scale bar: 100 μm).

capability based on triple shape memory effect. The inadequate shape recovery was in accordance with the quantitatively calculated results of the shape recovery ratio. This may be due to unintended shape change caused by repetitive programming procedure in a shape memory cycle, which was common in triple SMPs and physically crosslinked SMPs [52].

3.5. Quintuple and selective shape transformation of 4D printed multi-material SMP

The introduction of Fe_3O_4 endowed the material with magnetic-responsive triple shape memory effect in an alternating magnetic field as illustrated in Fig. 6(a) and Movie S2 (Supporting Information). Upon continuous 30 kHz alternating magnetic field heating, the predeformed tetrahedron unfolded into the programmed temporary shape and the original shape successively. Since both PLMC/PTMC and PLMC/PTMC/Fe_3O_4 had triple-shape memory effect, each part of the printed structure could memorize two temporary shapes. Fig. 6(b) demonstrates a series of selective shape recovery processes of the 4D printed multi-material crane. The original shape (S0) was folded into two temporary shapes (S1 and S2) where only the wings were deformed in a water bath at 70 and 45 ℃, respectively. Then it was programmed into another two shapes (S3 and S4) where the body of the crane was put flat in a magnetic field. When it was subjected to the magnetic field again, only the zone containing Fe_3O_4 was magnetic-responsive and thus recovered to the predeformed shapes ($S3_{rec}$ and $S2_{rec}$) sequentially as shown in Movie S3 (Supporting Information). Then by immersing in a water bath at 45 and 70 ℃, the non-magnetic-responsive zone achieved partial and full shape recovery to $S1_{rec}$ and $S0_{rec}$, respectively. Fig. 6(c) illustrates a similar multiple shape change of the 4D printed multi-material flower under both the magnetic and thermal response. In the whole process, five complex shapes and multiple shape transformations were simply realized by multi-material 4D printing of SMP and its composites, exhibiting potential for applications that required both complex shapes and specific external stimuli.

3.6. Biocompatibility of 4D printed multiple-SMP

The CCK-8 assay shown in Fig. 7(a) was adopted to determine the effect of printed PLMC/PTMC on the growth of fibroblast cells within 3 days. The 3D printed material demonstrated no influence on the cell viability of NIH/3T3 fibroblast cells, both in the dose- and time-dependent manner. The result showed there was no statistical difference in different groups. The LIVE/DEAD Cytotoxicity assay was also detected in which lived and dead cells were stained with green and red fluorescence, respectively. The 3D printed monolayer possessed ultra-thin nature to allow for the passage of light used for imaging the cells in the assay. In Fig. 7(b), the result of the LIVE/DEAD assay as shown in Fig. 7(b) indicates that at all printed films support cells growth. Almost all the detected cells were live as inducted by the green color, with very few dead cells detected in all the scaffolds after 48 h. It reflected that the 3D printed multiple-SMP and its nanocomposites were less cytotoxic to fibroblast cells, proving they were optimal for supporting cell growth. Besides, both PLMC and PTMC have been proved as promising biomaterial with high attachment and proliferation with human cells, displaying adequate material-cell interactions [53,54]. Besides, as magnetic particles, Fe_3O_4 are highly biocompatible [55]. Adding them into biocompatible polymers enables non-contacting remote actuation, which has been widely used in many biomedical applications [56]. Furthermore, 4D printed SMP structures could be programmed into small temporary shapes and then expand upon stimuli, which is helpful for minimally invasive surgery to reduce the surgical wound area [51, 57]. Thus it could be expected that our biocompatible and nontoxic 4D printed nanocomposites will show great prospects for biomedical applications.

Based on the material design and biocompatible 4D printed shape-changing structures, we envision three promising applications as follows. First, the shape transformation from one temporary shape to quintuple complex shapes with accurately and locally controllability under various selectivestimuli is promising for fashion and entertainment industry. The self-blooming flower and self-folding crane illustrate the combination of the 4D printed origami with multiple shape memory, creating more freedom of programming and providing more design space for the fashion and entertainment field. Second, the self-folding tetrahedron and self-blooming flower have demonstrated the potential of this technology to be applied as a smart gripper. For example, the closure of the petals may grab some loads under heat or magnetic field. Third, 4D printed biodegradable material show promise as self-expanding stents which could be helpful for minimally invasive surgery to reduce the surgical wound area.

4. Conclusion

In summary, we propose a feasible paradigm to construct 4D printed multi-material consisting of triple SMP and its nanocomposites by direct ink writing. Initially, we optimize the best properties of triple SMP with various compositions of PLMC/PTMC. The material design demonstrates excellent repeatability and reliability in consecutive shape memory cycles. Then we introduce the Fe_3O_4 nanoparticles to the triple SMP to possess remotely magnetic-responsive and complicated shape

transformation with more degrees of freedom. By integrating multi-material design and triple shape memory response, the developed method allows for the fabrication of 4D printed structures with locally controllable sequential shape change under selective stimuli of magnetic field and heat. The 4D printed triple-SMP and its nanocomposites also exhibit excellent biocompatibility. This feasible method represents an important step forward for the advanced additive manufacturing of biocompatible 4D printed triple-SMP and multi-material, demonstrating great potential for biomedical applications such as drug delivery and tissue engineering, etc.

CRediT authorship contribution statement

Xue Wan: Writing – review & editing, Writing – original draft, Visualization, Methodology, Formal analysis, Data curation, Conceptualization. **Yang He:** Writing – review & editing, Supervision, Data curation, Conceptualization. **Yanju Liu:** Writing – review & editing, Supervision, Resources, Project administration, Funding acquisition, Conceptualization. **Jinsong Leng:** Writing – review & editing, Supervision Resources, Project administration, Funding acquisition, Conceptualization..

Declaration of Competing Interest

The authors declare that they have no known competing financial interests or personal relationships that could have appeared to influence the work reported in this paper.

Acknowledgments

This work has been supported by the National Natural Science Foundation of China (Grant Nos. 11632005, 12072094 and 12172106) and the Heilongjiang Touyan Innovation Team Program, for which we are very grateful.

Appendix A. Supporting information

Supplementary data associated with this article can be found in the online version at doi:10.1016/j.addma.2022.102689.

References

[1] K. Fu, Y. Yao, J. Dai, L. Hu, Progress in 3D printing of carbon materials for energy-related applications, Adv. Mater. 29 (2017) 1603486, https://doi.org/10.1002/adma.201603486.
[2] S. Bose, D. Ke, H. Sahasrabudhe, A. Bandyopadhyay, Additive manufacturing of biomaterials, Prog. Mater. Sci. 93 (2018) 45–111, https://doi.org/10.1016/j.pmatsci.2017.08.003.
[3] N. Guo, M.C. Leu, Additive manufacturing: technology, applications and research needs, Front. Mech. Eng. 8 (2013) 215–243, https://doi.org/10.1007/s11465-013-0248-8.
[4] S.C. Joshi, A.A. Sheikh, 3D printing in aerospace and its long-term sustainability, Virtual Phys. Prototyp. 10 (2015) 175–185, https://doi.org/10.1080/17452759.2015.1111519.
[5] S. Tibbits, 4D printing: multi-material shape change, Archit. Des. 84 (2014) 116–121, https://doi.org/10.1002/ad.1710.
[6] A.S. Gladman, E.A. Matsumoto, R.G. Nuzzo, L. Mahadevan, J.A. Lewis, Biomimetic 4D printing, Nat. Mater. 15 (2016) 413, https://doi.org/10.1038/nmat4544.
[7] L.M. Huang, R.Q. Jiang, J.J. Wu, J.Z. Song, H. Bai, B.G. Li, Q. Zhao, T. Xie, Ultrafast digital printing toward 4D shape changing materials, Adv. Mater. 29 (2017) 1605390, https://doi.org/10.1002/adma.201605390.
[8] X. Kuang, D.J. Roach, J.T. Wu, C.M. Hamel, Z. Ding, T.J. Wang, M.L. Dunn, H.J. Qi, Advances in 4D printing: materials and applications, Adv. Funct. Mater. 29 (2019) 1805290, https://doi.org/10.1002/adfm.201805290.
[9] S.D. Miao, N. Castro, M. Nowicki, L. Xia, H.T. Cui, X. Zhou, W. Zhu, S.J. Lee, K. Sarkar, G. Vozzi, Y. Tabata, J. Fisher, L.G. Zhang, 4D printing of polymeric materials for tissue and organ regeneration, Mater. Today 20 (2017) 577–591, https://doi.org/10.1016/j.mattod.2017.06.005.
[10] C.M. Gonzalez-Henriquez, M.A. Sarabia-Vallejos, J. Rodriguez-Hernandez, Polymers for additive manufacturing and 4D-printing: Materials, methodologies, and biomedical applications, Prog. Polym. Sci. 94 (2019) 57–116, https://doi.org/10.1016/j.progpolymsci.2019.03.001.
[11] H. Wu, X. Zhang, Z. Ma, C. Zhang, J. Ai, P. Chen, C. Yan, B. Su, Y. Shi, A material combination concept to realize 4D printed products with newly emerging property/functionality, Adv. Sci. 7 (2020) 1903208, https://doi.org/10.1002/advs.201903208.
[12] A. Lendlein, S. Kelch, Shape-memory polymers, Angew. Chem. Int Ed. 41 (2002) 2034–2057, https://doi.org/10.1002/1521-3773(20020617)41:12<2034::AID-ANIE2034>3.0.CO;2-M.
[13] M. Behl, A. Lendlein, Shape-memory polymers, Mater. Today 10 (2007) 20–28, https://doi.org/10.1016/S1369-7021(07)70047-0.
[14] J.S. Leng, X. Lan, Y.J. Liu, S.Y. Du, Shape-memory polymers and their composites: stimulus methods and applications, Prog. Mater. Sci. 56 (2011) 1077–1135, https://doi.org/10.1016/j.pmatsci.2011.03.001.
[15] C. Liu, H. Qin, P.T. Mather, Review of progress in shape-memory polymers, J. Mater. Chem. 17 (2007) 1543–1558, https://doi.org/10.1039/B615954K.
[16] W.M. Sokolowski, S.C. Tan, Advanced self-deployable structures for space applications, J. Spacecr. Rocket. 44 (2007) 750–754, https://doi.org/10.2514/1.22854.
[17] J. Zhang, C. Wang, L. Zhang, Deployment of SMP Miura-ori sheet and its application: aerodynamic drag and RCS reduction, Chin. J. Aeronaut. (2021), https://doi.org/10.1016/j.cja.2021.08.004.
[18] G. Ugur, J.Y. Chang, S.H. Xiang, L.W. Lin, J. Lu, A near-infrared mechano responsive polymer system, Adv. Mater. 24 (2012) 2685–2690, https://doi.org/10.1002/adma.201104538.
[19] J. Shintake, V. Cacucciolo, D. Floreano, H. Shea, Soft robotic grippers, Adv. Mater. 30 (2018) 1707035, https://doi.org/10.1002/adma.201707035.
[20] M. Zarek, M. Layani, I. Cooperstein, E. Sachyani, D. Cohn, S. Magdassi, 3D printing of shape memory polymers for flexible electronic devices, Adv. Mater. 28 (2016) 4449–4454, https://doi.org/10.1002/adma.201503132.
[21] A. Lendlein, R. Langer, Biodegradable, elastic shape-memory polymers for potential biomedical applications, Science 296 (2002) 1673–1676, https://doi.org/10.1126/science.1066102.
[22] K. Yu, A. Ritchie, Y. Mao, M.L. Dunn, H.J. Qi, Controlled sequential shape changing components by 3D printing of shape memory polymer multimaterials, Procedia IUTAM 12 (2015) 193–203, https://doi.org/10.1016/j.piutam.2014.12.021.
[23] Q. Ge, A.H. Sakhaei, H. Lee, C.K. Dunn, N.X. Fang, M.L. Dunn, Multimaterial 4D printing with tailorable shape memory polymers, Sci. Rep. 6 (2016) 31110, https://doi.org/10.1038/srep31110.
[24] T. Xie, Recent advances in polymer shape memory, Polymer 52 (2011) 4985–5000, https://doi.org/10.1016/j.polymer.2011.08.003.
[25] A. Lendlein, O.E.C. Gould, Reprogrammable recovery and actuation behaviour of shape-memory polymers, Nat. Rev. Mater. 4 (2019) 116–133, https://doi.org/10.1038/s41578-018-0078-8.
[26] T. Xie, Tunable polymer multi-shape memory effect, Nature 464 (2010) 267–270, https://doi.org/10.1038/nature08863.
[27] J. Li, T. Liu, S. Xia, Y. Pan, Z. Zheng, X. Ding, Y. Peng, A versatile approach to achieve quintuple-shape memory effect by semi-interpenetrating polymer networks containing broadened glass transition and crystalline segments, J. Mater. Chem. 21 (2011) 12213–12217, https://doi.org/10.1039/C1JM12496J.
[28] C. Samuel, S. Barrau, J.M. Lefebvre, J.M. Raquez, P. Dubois, Designing multiple-shape memory polymers with miscible polymer blends: evidence and origins of a triple-shape memory effect for miscible PLLA/PMMA blends, Macromolecules 47 (2014) 6791–6803, https://doi.org/10.1021/ma500846x.
[29] J.J. Li, T. Xie, Significant impact of thermo-mechanical conditions on polymer triple-shape memory effect, Macromolecules 44 (2011) 175–180, https://doi.org/10.1021/ma102279y.
[30] Y. Luo, Y. Guo, X. Gao, B.-G. Li, T. Xie, A general approach towards thermoplastic multishape-memory polymers via sequence structure design, Adv. Mater. 25 (2013) 743–748, https://doi.org/10.1002/adma.201202884.
[31] W. Li, Y. Liu, J. Leng, Selectively actuated multi-shape memory effect of a polymer multicomposite, J. Mater. Chem. A 3 (2015) 24532–24539, https://doi.org/10.1039/C5TA08513F.
[32] S. Chen, J. Hu, C.-W. Yuen, L. Chan, H. Zhuo, Triple shape memory effect in multiple crystalline polyurethanes, Polym. Adv. Technol. 21 (2010) 377–380, https://doi.org/10.1002/pat.1523.
[33] Q. Guan, B. Norder, L. Chu, N.A.M. Besseling, S.J. Picken, T.J. Dingemans, All-aromatic (AB)n-multiblock copolymers via simple one-step melt condensation chemistry, Macromolecules 49 (2016) 8549–8562, https://doi.org/10.1021/acs.macromol.6b01341.
[34] G. Li, A. King, T. Xu, X. Huang, Behavior of thermoset shape memory polymer-based syntactic foam sealant trained by hybrid two-stage programming, J. Mater. Civ. Eng. 25 (2013) 393–402, https://doi.org/10.1061/(ASCE)MT.1943-5533.0000572.
[35] G. Li, A. Wang, Cold, warm, and hot programming of shape memory polymers, J. Polym. Sci., Part B: Polym. Phys. 54 (2016) 1319–1339, https://doi.org/10.1002/polb.24041.
[36] H. Li, X. Gao, Y. Luo, Multi-shape memory polymers achieved by the spatio-assembly of 3D printable thermoplastic building blocks, Soft Matter 12 (2016) 3226–3233, https://doi.org/10.1039/C6SM00185H.
[37] S. Chen, Q. Zhang, J. Feng, 3D printing of tunable shape memory polymer blends, J. Mater. Chem. C. 5 (2017) 8361–8365, https://doi.org/10.1039/C7TC02534C.
[38] L.R. Lopes, A.F. Silva, O.S. Carneiro, Multi-material 3D printing: the relevance of materials affinity on the boundary interface performance, Addit. Manuf. 23 (2018) 45–52, https://doi.org/10.1016/j.addma.2018.06.027.
[39] X. Wan, L. Luo, Y. Liu, J. Leng, Direct ink writing based 4D printing of materials and their applications, Adv. Sci. 7 (2020) 2001000, https://doi.org/10.1002/advs.202001000.

[40] M. Rafiee, R.D. Farahani, D. Therriault, Multi-material 3D and 4D printing: a survey, Adv. Sci. 7 (2020) 1902307, https://doi.org/10.1002/advs.201902307.
[41] R. Dolog, R.A. Weiss, Shape memory behavior of a polyethylene-based carboxylate ionomer, Macromolecules 46 (2013) 7845–7852, https://doi.org/10.1021/ma401631j.
[42] T.P. Lodge, T.C.B. McLeish, Self-concentrations and effective glass transition temperatures in polymer blends, Macromolecules 33 (2000) 5278–5284, https://doi.org/10.1021/ma9921706.
[43] M.G. Abiad, O.H. Campanella, M.T. Carvajal, Assessment of thermal transitions by dynamic mechanical analysis (DMA) using a novel disposable powder holder, Pharmaceutics 2 (2010) 78–90, https://doi.org/10.3390/pharmaceutics2020078.
[44] J. Xu, W. Shi, W. Pang, Synthesis and shape memory effects of Si–O–Si cross-linked hybrid polyurethanes, Polymer 47 (2006) 457–465, https://doi.org/10.1016/j.polymer.2005.11.035.
[45] N. Mhlanga, S. Sinha Ray, Y. Lemmer, J. Wesley-Smith, Polylactide-based magnetic spheres as efficient carriers for anticancer drug delivery, ACS Appl. Mat. Interfaces 7 (2015) 22692–22701, https://doi.org/10.1021/acsami.5b07567.
[46] K. Kratz, S.A. Madbouly, W. Wagermaier, A. Lendlein, Temperature-memory polymer networks with crystallizable controlling units, Adv. Mater. 23 (2011) 4058–4062, https://doi.org/10.1002/adma.201102225.
[47] T. Xie, K.A. Page, S.A. Eastman, Strain-based temperature memory effect for nafion and its molecular origins, Adv. Funct. Mater. 21 (2011) 2057–2066, https://doi.org/10.1002/adfm.201002579.
[48] P. Miaudet, A. Derré, M. Maugey, C. Zakri, P.M. Piccione, R. Inoubli, P. Poulin, Shape and temperature memory of nanocomposites with broadened glass transition, Science 318 (2007) 1294, https://doi.org/10.1126/science.1145593.
[49] Z.Y. Zhao, F. Peng, K.A. Cavicchi, M. Cakmak, R.A. Weiss, B.D. Vogt, Three-dimensional printed shape memory objects based on an olefin lonomer of zinc-neutralized poly(ethylene-co-emethacrylic acid), ACS Appl. Mat. Interfaces 9 (2017) 27239–27249, https://doi.org/10.1021/acsami.7b07816.
[50] J.E. Smay, J. Cesarano, J.A. Lewis, Colloidal Inks for directed assembly of 3-D periodic structures, Langmuir 18 (2002) 5429–5437, https://doi.org/10.1021/la0257135.
[51] C. Lin, J. Lv, Y. Li, F. Zhang, J. Li, Y. Liu, L. Liu, J. Leng, 4D-printed biodegradable and remotely controllable shape memory occlusion devices, Adv. Funct. Mater. 29 (2019) 1906569, https://doi.org/10.1002/adfm.201906569.
[52] Q. Zhao, H.J. Qi, T. Xie, Recent progress in shape memory polymer: new behavior, enabling materials, and mechanistic understanding, Prog. Polym. Sci. 49–50 (2015) 79–120, https://doi.org/10.1016/j.progpolymsci.2015.04.001.
[53] A.P. Pego, B. Siebum, M.J.A. Van Luyn, X.J.G.Y. Van Seijen, A.A. Poot, D. W. Grijpma, J. Feijen, Preparation of degradable porous structures based on 1,3-trimethylene carbonate and D,L-lactide (co)polymers for heart tissue engineering, Tissue Eng. 9 (2003) 981–994, https://doi.org/10.1089/107632703322495628.
[54] S. Schüller-Ravoo, E. Zant, J. Feijen, D.W. Grijpma, Preparation of a designed poly (trimethylene carbonate) microvascular network by Stereolithography, Adv. Healthc. Mater. 3 (2014) 2004–2011, https://doi.org/10.1002/adhm.201400363.
[55] J. Sun, S. Zhou, P. Hou, Y. Yang, J. Weng, X. Li, M. Li, Synthesis and characterization of biocompatible Fe3O4 nanoparticles, J. Biomed. Mater. Res. Part A 80A (2007) 333–341, https://doi.org/10.1002/jbm.a.30909.
[56] P.R. Buckley, G.H. Mckinley, T.S. Wilson, W. Small, W.J. Benett, J.P. Bearinger, M. W. Mcelfresh, D.J. Maitland, Inductively heated shape memory polymer for the magnetic actuation of medical devices, IEEE Trans. Biomed. Eng. 53 (2006) 2075–2083, https://doi.org/10.1109/TBME.2006.877113.
[57] W. Zhao, Z. Huang, L. Liu, W. Wang, J. Leng, Y. Liu, Porous bone tissue scaffold concept based on shape memory PLA/Fe3O4, Compos. Sci. Technol. 203 (2021), 108563, https://doi.org/10.1016/j.compscitech.2020.108563.